ADVANCED FUNCTIONAL MATERIALS

FULL PAPER

DOI: 10.1002/adfm.200800625

High Purity GaAs Nanowires Free of Planar Defects: Growth and Characterization**

By *Hannah J. Joyce,* Qiang Gao, H. Hoe Tan, Chennupati Jagadish, Yong Kim, Melodie A. Fickenscher, Saranga Perera, Thang Ba Hoang, Leigh M. Smith, Howard E. Jackson, Jan M. Yarrison-Rice, Xin Zhang,* and *Jin Zou*

We investigate how to tailor the structural, crystallographic and optical properties of GaAs nanowires. Nanowires were grown by Au nanoparticle-catalyzed metalorganic chemical vapor deposition. A high arsine flow rate, that is, a high ratio of group V to group III precursors, imparts significant advantages. It dramatically reduces planar crystallographic defects and reduces intrinsic carbon dopant incorporation. Increasing V/III ratio further, however, instigates nanowire kinking and increases nanowire tapering. By choosing an intermediate V/III ratio we achieve uniform, vertically aligned GaAs nanowires, free of planar crystallographic defects, with excellent optical properties and high purity. These findings will greatly assist the development of future GaAs nanowire-based electronic and optoelectronic devices, and are expected to be more broadly relevant to the rational synthesis of other III–V nanowires.

1. Introduction

Semiconductor nanowires hold outstanding potential as nano-components of future devices and systems. A wide range of nanowire based electronic and photonic devices have already been built, including nanowire solar cells,[1] lasers,[2] photodetectors,[3] single-electron memory devices,[4] and DNA detectors.[5] Several of these devices were created using III–V nanowires, which are especially promising owing to the superior electrical and optical properties of III–V materials. Epitaxial III–V nanowires may be fabricated in a potentially scalable, flexible and well-controlled manner, via metalorganic chemical vapor deposition (MOCVD) according to a Au nanoparticle assisted vapor–liquid–solid (VLS)[6] or vapor–solid–solid (VSS) mechanism.[7]

Amongst semiconductor nanowires, GaAs nanowires have significant merits associated with the direct band gap and high electron mobility of the GaAs material system. The GaAs material system is used extensively in the electronics and optoelectronics industries, and accordingly GaAs nanowires are prime candidates for electrically and optically active nanowire devices such as lasers and photodetectors.[8] In this study we investigate how to tailor GaAs nanowire growth to obtain GaAs nanowires with device accessible properties. Furthermore, the growth of III–V nanowires such as GaAs and InP, is governed by common principles.[9] Therefore, we anticipate that many of our findings are not specific to GaAs nanowires, but are broadly applicable to other III–V nanowire systems.

If GaAs nanowires are to be useful in optoelectronic devices, they require excellent crystallographic and optical qualities. Furthermore, integrated nanowire device architectures[10] generally demand straight nanowires with well-controlled orientation. Therefore, crystallographic defects, notably twinning,[11] and nanowire kinking, are two major growth issues to overcome.[12] Additionally, the unintentional incorporation of dopant impurities such as carbon gives rise to electronic energy levels within the band gap, which can adversely affect the optical and electronic properties of these

[*] H. J. Joyce, Dr. Q. Gao, Dr. H. H. Tan, Prof. C. Jagadish
Department of Electronic Materials Engineering
Research School of Physical Sciences and Engineering
The Australian National University, Canberra ACT 0200 (Australia)
E-mail: hjj109@rsphysse.anu.edu.au
Prof. Y. Kim
Department of Physics, Dong-A University
Hadan-2-dong, Sahagu, Busan 604-714 (Korea)
M. A. Fickenscher, S. Perera, Dr. T. B. Hoang, Prof. L. M. Smith
Prof. H. E. Jackson
Department of Physics, University of Cincinnati
Cincinnati, Ohio OH 45221 (USA)
Prof. J. M. Yarrison-Rice
Department of Physics, Miami University
Oxford, Ohio OH 45056 (USA)
Dr. X. Zhang, Prof. J. Zou
School of Engineering and Centre for Microscopy and Microanalysis
The University of Queensland
Brisbane QLD 4072 (Australia)

[**] We thank the Australian Research Council, the National Science Foundation (Grants ECCS-0701703 and DMR-0806700) and the Korean Science and Engineering Foundation (Grant NO. F01-2007-000-10087-0) for financial support. HJJ thanks the Australian Research Council Nanotechnology Network for an overseas travel fellowship to enable her collaborative visit to the University of Cincinnati. The Australian National Fabrication Facility established under the Australian Government's National Collaborative Research Infrastructure Strategy, is gratefully acknowledged for providing access to the facilities used in this research.

ADVANCED FUNCTIONAL MATERIALS

nanowires. To date there have been only limited reports in the literature on intrinsic dopant incorporation in GaAs nanowires.[13] Controlling intrinsic doping is critical for producing high purity nanowires.

Recently high quality nanowires have been produced by controlling growth temperature,[12] and the temperature dependencies of GaAs nanowire growth are well-reported.[14,15] Here we explore another key growth parameter: the flow rate of the group V precursor species, arsine. This is equivalent to studying the ratio of group V precursor flow rate to group III precursor flow rate, that is, V/III ratio. In the present literature there are only limited reports of the effects of this important growth parameter.[6,15] We demonstrate how V/III ratio affords precise control over crystallographic defect density and impurity incorporation. We find that a high V/III ratio can achieve nanowires that are free of crystallographic defects. These nanowires also give strong excitonic emission with minimal impurity-related emission, indicating their high purity. We identify carbon as the dominant acceptor impurity in GaAs nanowires. The highest V/III ratios, however, produce nanowires with undesirable kinked and tapered morphologies. This places an upper limit on the range of useful V/III ratios. We determine that an intermediate V/III ratio gives optimum nanowire properties. Further, these effects of V/III ratio yield important information on the mechanisms of kinking, twin formation and carbon impurity incorporation.

2. Results and Discussion

In this study, nanowires were grown on semi-insulating GaAs (111)B substrates using trimethylgallium (TMG) and AsH_3 precursors. We studied the effect of V/III ratio by varying the group V (AsH_3) flow rate while holding the group III (TMG) flow rate constant. The control TMG flow rate, denoted III_0, was 1.2×10^{-5} mol min^{-1} and AsH_3 flow rates were chosen between 1.3×10^{-4}–2.1×10^{-3} mol min^{-1} to attain V/III ratios of 12, 23, 46, 93, and 190.

Adjunct studies were performed with other TMG flow rates: $\frac{1}{4}$ III_0, $\frac{1}{2}$ III_0, 2 III_0, and 4 III_0 spanning TMG flow rates of 2.9×10^{-6}– 4.6×10^{-5} mol min^{-1}. In each study, TMG was held constant and AsH_3 was varied to achieve a given V/III ratio.

GaAs nanowires grown under various V/III conditions have been characterized by field emission scanning electron microscopy (FESEM), transmission electron microscopy (TEM) and low temperature time-integrated and time-resolved photoluminescence (PL) measurements. PL represents a convenient, contact-free method of determining the electronic and impurity states in bulk GaAs[16] and in semiconductor nanostructures such as these GaAs nanowires.[17,18] For PL measurements, nanowires were clad in AlGaAs shells to passivate the nanowire surface and hence improve PL emission.[17] The results of these studies are discussed below.

2.1. Morphology

The V/III ratio has a profound effect on nanowire morphology, particularly the nanowire growth direction. Figure 1 illustrates nanowires grown with $III = III_0$ and various V/III ratios. At low V/III ratios, illustrated in Figure 1a–c, nanowire growth initiates in the vertical [111]B direction and this epitaxial growth continues in this direction to create straight vertically oriented nanowires. At a critical V/III ratio of approximately 90 (Fig. 1d), however, a small proportion of nanowires kink to a non-vertical orientation during growth. At even higher V/III ratio (Fig. 1e) the proportion of kinked nanowires increases. Dayeh et al.[19] have made similar observations, reporting InAs nanowires growing at angles to the substrate normal at high V/III ratios.

Nanowire tapering, whereby nanowires exhibit a larger diameter at the nanowire base and a narrower diameter at the Au-capped nanowire tip, is another morphological feature of significance for device applications.[12] With increasing V/III ratio, nanowire tapering increases slightly as shown in Figure 1. This is consistent with previous reports and is explained as follows.[19,20] The activation energy for two dimensional planar growth is known to decrease with increasing V/III ratio.[21] Consequently, the two dimensional, that is, radial, growth rate increases with V/III ratio,[19,20] resulting in more tapered nanowires.

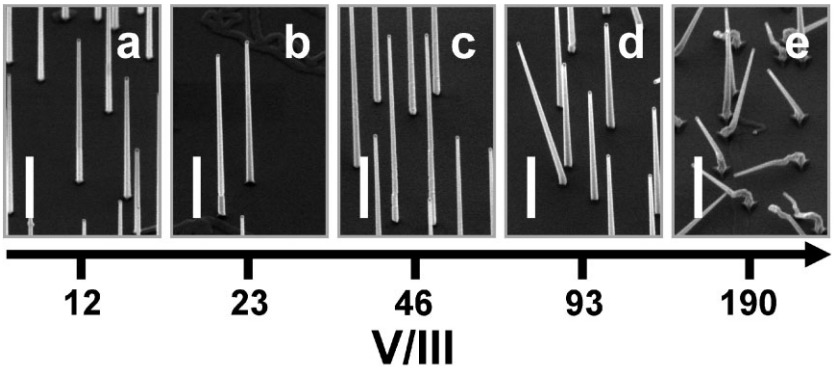

Figure 1. FESEM images of nanowires grown at constant $III = III_0$ and indicated V/III ratios: a) 12, b) 23, c) 46, d) 93, and e) 190. Axis is logarithmic. Scale bars are 1 μm. Samples are tilted at 40°.

Nanowire lengths, too, vary with V/III ratio, in agreement with previous reports.[6,15,19,22,23] In the range of low V/III ratios, approximately 46 and below (Fig. 1a–c), we observe a distinct trend. Here the axial growth rate increases with increasing V/III ratio, and taller nanowires result. In the range of high V/III ratios, approximately 46 and above (Fig. 1c and d), the opposite effect is observed. Here the vertical growth rate decreases with increasing V/III ratio, and shorter nanowires result.

In the low V/III ratio range, the observed result is expected because AsH_3 reaction

species enhance the decomposition of TMG.[24] This leads to a higher axial growth rate and taller nanowires with increasing AsH_3 flow rate.[15] In the high V/III ratio range, there are two factors which may contribute to the observation of decreasing axial growth rate with increasing V/III ratio. First, at higher V/III ratios, the radial growth rate increases as described above. Ga adatoms, diffusing from the substrate and along the nanowire sidewalls towards the growing Au-capped nanowire tip, are consumed by this radial growth. These Ga adatoms would otherwise diffuse to the nanowire tip and contribute to axial growth. In short, radial growth competes with axial growth for these Ga adatoms.[14] Therefore, with increasing V/III ratio, the increase in radial growth rate produces a decrease in axial growth rate.[19] Second, at high AsH_3 flows, stable As trimers are known to form on As-terminated (111)B surfaces.[25] Ikejeri et al.[23] have proposed, in the case of catalyst-free GaAs nanowires, that this surface reconstruction hinders growth on the (111)B nanowire surface.[26] The growth rate in the vertical [111]B direction therefore becomes low with increasing AsH_3 flow rate.[23]

Perhaps most interesting is the observation of kinking. For all III flows investigated, the onset of kinking occurred at a critical V/III ratio of approximately 90. The dependence of kinking on V/III ratio indicates that TMG counteracts the kink-producing effects of AsH_3.

One possible reason behind nanowire kinking, is that high V/III ratios change surface energies to favor other growth directions. As discussed above, at high AsH_3 flows, stable As trimers form on As-terminated (111)B surfaces. In our case of Au-assisted nanowire growth, this surface reconstruction could not only decrease the [111]B growth rate, but could also favor a growth direction other than [111]B, causing nanowire growth to kink to a non-[111]B direction.

A second possible factor is that complete or partial solidification of the Au nanoparticle drives kinked irregular growth.[12] Under this suggestion, Ga supplied from TMG decomposition dissolves into the Au nanoparticle and promotes the liquid eutectic state of the Au nanoparticle.[27] As discussed above, a high V/III ratio promotes radial growth. Radial growth consumes Ga adatoms which would otherwise reach the Au nanoparticle-capped nanowire tip, and consequently depletes the nanoparticle of Ga.[19] This in turn can prevent the formation of the eutectic liquid nanoparticle, and can instead favor a solid nanoparticle at high V/III ratios. With a solid nanoparticle, we might also expect the growth rate to decrease[28] leading to shorter nanowires. Indeed, the vertical nanowires of Figure 1d, grown at high V/III ratio, are shorter than those of Figure 1a–c.

The two kinking mechanisms discussed above may both play a role, and neither mechanism precludes the other. Furthermore, these results suggest that a high V/III ratio can be used to select a growth direction other than [111]B, potentially another well-defined crystallographic direction. This would offer a novel and simple means of creating branched nanowires[29] and three-dimensional networks of interconnected nanowires,[30] without requiring more complex sequential seeding methods.[29]

We note that nanowire kinking and tapering, induced by the highest V/III ratios, are potentially deleterious for practical nanowire applications. The onset of kinking and severe tapering will place an upper limit on the range of useful V/III ratios.

2.2. Crystallographic Properties

We now turn to nanowire crystallographic properties as a function of V/III ratio. All nanowires were of zinc blende crystal structure. Twins are common lattice defects in GaAs and other zinc blende III–V nanowires,[11,31] and can degrade the performance of optoelectronic nanowire devices. Indeed, non-periodic twin defects are apparent in Figure 2a, a TEM image of a nanowire grown with a low V/III ratio of 12. Figure 2b, on the other hand, illustrates a twin-free nanowire grown with a high V/III ratio of 93.

We defined twin density as the average number of twins per unit length of nanowire, and plotted twin density versus V/III ratio in Figure 2c. Figure 2c contains 4 data sets each corresponding to a constant III flow. For each III flow, increasing the AsH_3 flow, and hence increasing the V/III ratio, decreases the twin density. This sensitivity to the V/III ratio is likely related to how AsH_3 changes the surface and interfacial energies of the Au nanoparticle–nanowire system, as discussed below.

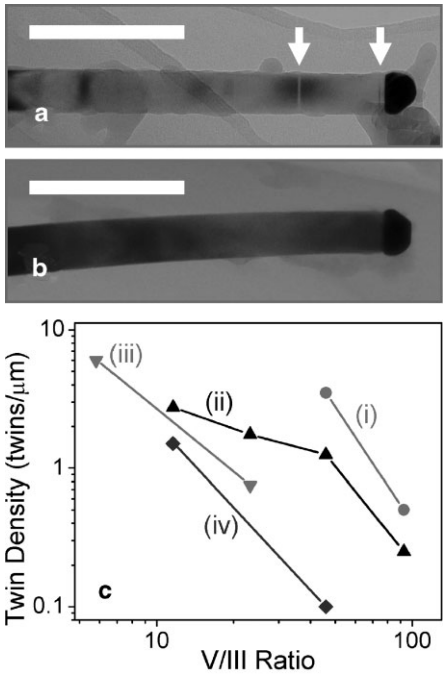

Figure 2. a) and b) Bright field TEM images of nanowires. a) Twinned nanowire grown at low V/III = 12 and III = III_0. Arrows indicate twin defects. b) Twin-free nanowire grown at high V/III = 93 and III = III_0. Scale bars are 250 nm. c) Twin density versus V/III ratio. Axes are logarithmic. Straight lines group data sets for a constant group III flow rate of (i) III = $\frac{1}{2}$ III_0, (ii) III = III_0, (iii) III = 2 III_0, and (iv) III = 4 III_0.

ADVANCED FUNCTIONAL MATERIALS

Surface and interfacial tension is believed to be a driving force behind twin formation in many nanowire[32,33] and bulk systems.[34] Studies have shown that during nanowire growth, each epitaxial plane nucleates at the three phase contact line, that is, the interface between the Au nanoparticle, the growing nanowire tip, and the ambient atmosphere.[31] Accordingly, twin plane nucleation initiates at the three phase contact line.[31] As nanowire growth progresses, nanowire side facets form,[31] the wettability and shape of the nanoparticle–nanowire interface may change,[32] and the nanoparticle may deform to wet this interface.[32] Consequently, surface and interfacial tensions at the three phase contact line may increase with continuing nanowire growth. Twin planes are thought to form to release this stored surface and interface energy.[32,33]

A surfactant, adsorbed on a surface or interface in the Au nanoparticle–nanowire system, can reduce the surface and interfacial tensions at the three phase contact line, and hence prevent the formation of twins. Arsenic species, with their very low solubility in gold,[35] are thought to act as surfactants[36] when adsorbed on the Au nanoparticle surface. Adsorbed As species would act to decrease the surface and interfacial tensions associated with the nanoparticle. Similar effects are observed with $AsCl_3$ in Au-catalyzed Ge whisker growth,[37] with excess As in melt growth of bulk GaAs,[34] and with As surfactant layers in epitaxial growth of island-free Si/Ge heterostructures.[36] Thus, by reducing surface and interfacial tensions, As species may decrease the incidence of twin defects in these GaAs nanowires.

Clearly, a dramatic decrease in twin density can be achieved using a high AsH_3 flow rate, that is, a high V/III ratio, as for the twin-free nanowire of Figure 2b. This is in marked contrast to the nanowire of Figure 2a grown at a low V/III ratio of 12, where a high twin density greater than 2 twins/μm is observed. It is noteworthy that the incidence of nanowire kinking (discussed in Sec. 2.1), unlike twin defects, increases with V/III ratio. This indicates that nanowire kinking and twin defects are unrelated and independent processes.

2.3. Photoluminescence

The optical properties of these nanowires were investigated using low temperature (18 K) micro-PL spectroscopy. PL spectra of Figure 3 were taken from a nanowire sample ($III = III_0$, $V/III = 46$) under different excitation intensities. These spectra feature two major peaks. The peak at approximately 1.517 eV[17] is characteristic of free exciton recombination in bulk GaAs.[17,38] The other lower energy peak (between 1.48 and 1.50 eV) is an impurity related band. With increasing excitation power the exciton peak broadens and undergoes a slight blue-shift. This is suggestive of the formation of an electron–hole plasma at higher excitation powers, a phenomenon recently observed in InP nanowires.[39] Also, with increasing excitation intensity the impurity peak saturates and the exciton peak becomes more intense.

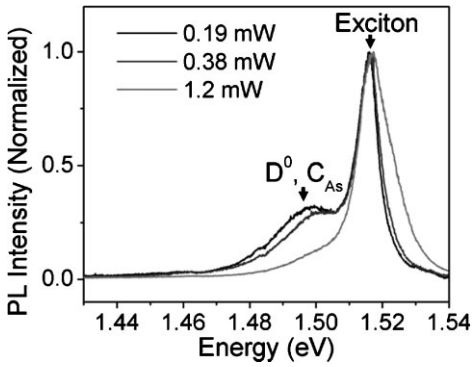

Figure 3. Normalized PL spectra from a typical nanowire ensemble (grown with $III = III_0$, $V/III = 46$) under different excitation intensities (indicated in legend). This illustrates the blue-shift and saturation of the impurity peak, and blue-shift with broadening of the exciton line, as excitation intensity increases.

The impurity related peak is assigned to donor–acceptor pair (DAP) recombination.[40] In Figure 4 we support this assignment by examining a nanowire sample ($III = \frac{1}{4}\, III_0$, $V/III = 46$) for which the impurity peak dominates the exciton peak. Figure 4a illustrates spectra for several excitation powers under continuous wave excitation. Figure 4b and c, respectively, illustrate time-resolved spectra at discrete time intervals after the excitation pulse, and time decays with corresponding lifetimes (τ) at various photon emission energies. According to Figure 4a the impurity emission band blue-shifts and narrows with increasing excitation power. This behavior is typical of DAP recombination.[41,42] Similar behavior is evident in the impurity emission peak of Figure 3. Further, time-resolved measurements are consistent with DAP recombination:[43] the peak red-shifts with time after the excitation pulse (Fig. 4b) and accordingly, higher emission energies have shorter lifetimes (Fig. 4c).

The DAP peak position closely corresponds to the position of neutral donor to neutral carbon acceptor (D^0, C_{As}) emission, reported at approximately 1.49 eV.[44] We therefore identify carbon as the dominant acceptor impurity in these GaAs nanowires, which is consistent with previous studies of MOCVD grown planar epitaxial GaAs layers[38,45] and GaAs nanowires.[13] We also note that, in studies of conventional planar epitaxy, the (111)B surface orientation exhibits the highest rate of carbon incorporation.[46] It is not unexpected, therefore, that these [111]B-oriented nanowires exhibit carbon impurity incorporation.

Each spectrum of Figure 4a features a smaller peak at lower energy than the main DAP peak. At all excitation intensities, this smaller peak maintains an approximately 36 meV energy separation below the DAP peak. This indicates the peak is a phonon replica of the DAP peak,[41] consistent with the 36 meV LO phonon energy.[47]

The exciton peak also shows an LO phonon replica at approximately 1.482 eV, as illustrated in Figure 3. The phonon replica is weaker for the exciton peak than for the DAP peak, possibly because the interaction between bound DAP charges

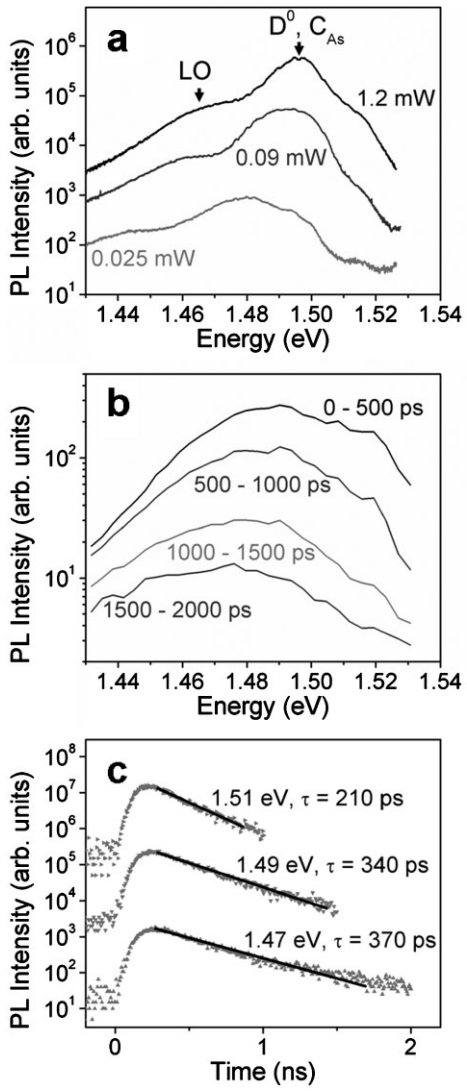

Figure 4. CW and time-resolved photoluminescence results obtained from a nanowire sample (grown with III = $\frac{1}{4}$ III$_0$, V/III = 46) with dominant impurity peak. a) CW PL spectra of a nanowire ensemble on semi-logarithmic axes illustrating blue-shift and narrowing of impurity peak with increasing excitation intensity. b) and c) Time-resolved PL measurements of a single nanowire. b) PL spectra integrated over consecutive 500 ps intervals after the excitation laser pulse. PL spectra red-shift with increasing time. c) Time decays at various emission energies. Time decays are offset for clarity and lifetimes (τ) are indicated.

and phonons may be enhanced relative to the interaction between free excitons and phonons. The relative intensity of the LO phonon replica, compared with the DAP peak, decreases with excitation intensity. This is consistent with the lower Huang–Rhys parameter for more closely spaced donor–acceptor pairs.[48]

Carbon is particularly problematic because it is the only impurity inherent in MOCVD growth of GaAs, arising as a decomposition product of TMG.[45] Other impurities such as Si and Zn can be eliminated using high purity precursor sources. For this reason it is important to choose growth parameters that minimize intrinsic carbon doping.

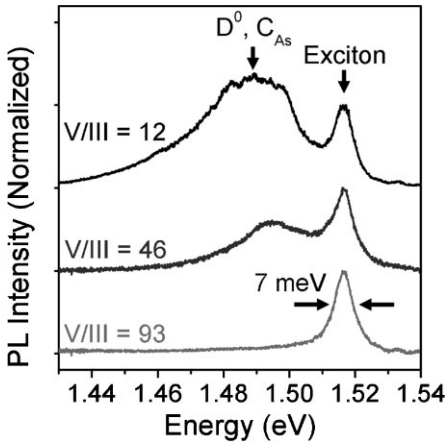

Figure 5. PL spectra comparing the relative intensities of DAP and exciton emission from nanowire ensembles with varying V/III ratios with constant III flow (III = III$_0$). The bottom-most spectrum features a FWHM of only 7 meV. Spectra are normalized to the exciton peak at 1.517 eV. Spectra are offset for clarity.

We use the relative intensity of the DAP peak to the exciton peak to gauge the degree of C impurity content, as has been reported in previous studies of C doped GaAs.[46,49] In Figure 5 we compare spectra for nanowires grown with various V/III ratios. These spectra were obtained under low excitation power (90 μW) to avoid saturation of the DAP peak. Spectra are normalized to the exciton peak at 1.517 eV. Clearly, the DAP peak intensity decreases with increasing V/III ratio. We infer that the C impurity density decreases with increasing V/III ratio.

This result parallels previous studies of background impurities in MOCVD grown planar epitaxial GaAs, which show that C acceptor impurities decrease with increasing V/III ratio.[38,46] C impurities arise from the adsorption of methyl (CH_3) radicals formed during the dissociation of TMG.[46,50] AsH_3 suppresses the adsorption of these CH_3 radicals: AsH_3 pyrolysis produces atomic hydrogen, which bonds with CH_3 radicals to produce the volatile methane (CH_4) reaction product. The CH_4 reaction product then leaves the reactor and removes the C bearing radical from the growth surface. Therefore higher AsH_3 flows, that is, higher V/III ratios, reduce C incorporation in nanowires. Thus nanowires of better purity and consequently superior optical quality can be achieved simply by choosing a high V/III ratio.

The bottom spectrum of Figure 5, taken from an ensemble of nanowires grown at a high V/III ratio of 93, shows little evidence of C-related emission. The spectrum is dominated by excitonic emission with a relatively narrow linewidth with a full width at half maximum (FWHM) of only 7 meV. Such a narrow linewidth is comparable to linewidths observed in high quality single InP nanowires.[51] The GaAs nanowires giving the bottom spectrum were predominantly free of twin defects, occasionally featuring one twin defect per nanowire of 3 μm total length. Images of the corresponding nanowire cores are displayed in Figures 1d and 2b. We have demonstrated that a

ADVANCED FUNCTIONAL MATERIALS

high V/III ratio not only favors high optical quality, but also minimizes twin defects. Increasing V/III ratio further, however, instigates severe nanowire kinking and tapering as discussed above and illustrated in Figure 1e. Therefore an intermediate V/III ratio achieves nanowires with optimal properties. In our system, we observe an intermediate V/III ratio of 93 produces nanowires predominantly oriented in the [111]B direction, with an acceptably small degree of tapering. These are generally free of planar defects and have excellent optical quality.

3. Conclusions

The development of nanowire based devices and systems depends on the ability to fabricate nanowires with tight control over properties such as morphology, crystal structure, optical properties and composition. We have demonstrated that GaAs nanowires of high optical and crystallographic quality may be achieved by choosing an appropriate group V precursor flow. A high V/III ratio markedly reduces the formation of twin defects and minimizes carbon impurity incorporation resulting in nanowires with excellent optical properties. The onset of nanowire kinking at the highest V/III ratios, together with the more significant nanowire tapering occurring at high V/III ratios, place an upper limit on the useful V/III ratio. An intermediate V/III ratio achieves straight, [111]B oriented epitaxial nanowires free of planar crystallographic defects and with minimal carbon impurity incorporation. High electron mobility can be expected in these twin-free nanowires. These findings will greatly assist the development of optoelectronic devices based on GaAs nanowires and associated nanowire heterostructures. Further, many of these results should translate to related nanowire materials systems such as InGaAs and AlGaAs.

4. Experimental

Growth: GaAs(111)B substrates were treated with poly-L-lysine (PLL) solution and a solution of colloidal 50 nm diameter Au nanoparticles, as described in previous reports. [52] Nanowires, catalyzed by these nanoparticles, were grown by horizontal flow MOCVD at a pressure of 100 mbar and a total gas flow rate of 15 slm. Prior to growth the substrate was annealed in situ at 600 °C under AsH_3 ambient to desorb surface contaminants. After cooling to a growth temperature of 450 °C TMG was introduced to initiate nanowire growth. For nanowire samples grown with $III = III_0$, growth time was 15 minutes. For other samples, growth time was scaled inversely with TMG flow. This was to achieve nanowires of reasonable height, at least 2 μm long and generally approximately 5 μm long, across all samples.

For PL measurements, GaAs nanowire cores were grown as described above, then clad in an AlGaAs shell to passivate the GaAs surface. [17,53] AlGaAs shell growth was performed for 20 minutes at 650 °C producing a shell approximately 30 nm thick with a nominal Al composition of 26%.

Electron Microscopy: FESEM images were obtained using a Hitachi S4500 with an accelerating voltage of 3 kV. TEM investigations were carried out using a FEI Tecnai F30. TEM specimens were prepared by ultrasonicating nanowire samples in ethanol for 20 minutes and then dispersing the nanowires onto holey carbon grids. Each data point of Figure 2c was determined by averaging the twin density of at least 3 nanowires.

Photoluminescence: AlGaAs clad nanowires were transferred from the as-grown GaAs substrate to Si substrates by gently touching the two substrates together. The Si substrate with dispersed nanowires was placed onto the cold finger of a variable temperature continuous flow helium cryostat. Measurements were conducted at 18 K using slit confocal micro-photoluminescence spectroscopy. A 50 × /0.5 NA long working distance microscope objective was used to project the PL image of the nanowire sample onto the entrance slit of the spectrometer. For time-integrated PL spectra, an ensemble of 5 to 10 nanowires was excited at 780 nm with a continuous wave Ti:S laser defocused to an approximately 10 μm diameter spot. Time-integrated PL was detected by a 2000 × 800 pixel liquid nitrogen cooled CCD detector. Time-resolved PL measurements were performed on single isolated nanowires using time correlated single photon counting, using pulsed laser excitation (780 nm, 800 μW) with 200 fs pulses at a 76 MHz repetition rate and a silicon avalanche photodiode detector. The temporal system response was measured to be 80 ps.

Received: May 5, 2008
Revised: June 20, 2008
Published online: September 22, 2008

[1] M. Law, L. E. Greene, J. C. Johnson, R. Saykally, P. Yang, *Nat. Mater.* **2005**, *4*, 455.
[2] a) M. H. Huang, S. Mao, H. Feick, H. Yan, Y. Wu, H. Kind, E. Weber, R. Russo, P. Yang, *Science* **2001**, *292*, 1897. b) X. F. Duan, Y. Huang, R. Agarwal, C. M. Lieber, *Nature* **2003**, *421*, 241.
[3] H. Pettersson, J. Trägårdh, A. I. Persson, L. Landin, D. Hessman, L. Samuelson, *Nano Lett.* **2006**, *6*, 229.
[4] C. Thelander, H. A. Nilsson, L. E. Jensen, L. Samuelson, *Nano Lett.* **2005**, *5*, 635.
[5] J.-I. Hahm, C. M. Lieber, *Nano Lett.* **2004**, *4*, 51.
[6] K. Hiruma, M. Yazawa, K. Haraguchi, K. Ogawa, T. Katsuyama, M. Koguchi, H. Kakibayashi, *J. Appl. Phys.* **1993**, *74*, 3162.
[7] K. A. Dick, K. Deppert, T. Mårtensson, B. Mandl, L. Samuelson, W. Seifert, *Nano Lett.* **2005**, *5*, 761.
[8] a) X. Duan, J. Wang, C. M. Lieber, *Appl. Phys. Lett.* **2000**, *76*, 1116. b) B. Hua, J. Motohisa, Y. Ding, S. Hara, T. Fukui, *Appl. Phys. Lett.* **2007**, *91*, 131112.
[9] K. A. Dick, K. Deppert, L. S. Karlsson, L. R. Wallenberg, L. Samuelson, W. Seifert, *Adv. Funct. Mater.* **2005**, *15*, 1603.
[10] a) H. T. Ng, J. Han, T. Yamada, P. Nguyen, Y. P. Chen, M. Meyyappan, *Nano Lett.* **2004**, *4*, 1247. b) M. S. Islam, S. Sharma, T. I. Kamins, R. S. Williams, *Nanotechnology* **2004**, *15*, L5.
[11] J. Zou, M. Paladugu, H. Wang, G. J. Auchterlonie, Y. Guo, Y. Kim, Q. Gao, H. J. Joyce, H. H. Tan, C. Jagadish, *Small* **2007**, *3*, 389.
[12] a) H. J. Joyce, Q. Gao, H. H. Tan, C. Jagadish, Y. Kim, X. Zhang, Y. Guo, J. Zou, *Nano Lett.* **2007**, *7*, 921. b) S. Perera, M. A. Fickenscher, H. E. Jackson, L. M. Smith, J. M. Yarrison-Rice, H. J. Joyce, Q. Goa, H. H. Tan, C. Jagadish, X. Zhang, J. Zou, *Appl. Phys. Lett.* **2008**, *93*, 053110.
[13] a) K. Hiruma, M. Yazawa, T. Katsuyama, K. Ogawa, K. Haraguchi, M. Koguchi, H. Kakibayashi, *J. Appl. Phys.* **1995**, *77*, 447. b) A. Mikkelsen, N. Sköld, L. Ouattara, E. Lundgren, *Nanotechnology* **2006**, *17*, S362.
[14] M. Borgström, K. Deppert, L. Samuelson, W. Seifert, *J. Cryst. Growth* **2004**, *260*, 18.
[15] M. A. Verheijen, G. Immink, T. de Smet, M. T. Borgström, E. P. A. M. Bakkers, *J. Am. Chem. Soc.* **2006**, *128*, 1353.

[16] D. J. Ashen, P. J. Dean, D. T. J. Hurle, J. B. Mullin, A. M. White, P. D. Greene, *J. Phys. Chem. Solids* **1975**, *36*, 1041.
[17] L. V. Titova, T. B. Hoang, H. E. Jackson, L. M. Smith, J. M. Yarrison-Rice, Y. Kim, H. J. Joyce, H. H. Tan, C. Jagadish, *Appl. Phys. Lett.* **2006**, *89*, 173126.
[18] T. B. Hoang, L. V. Titova, J. M. Yarrison-Rice, H. E. Jackson, A. O. Govorov, Y. Kim, H. J. Joyce, H. H. Tan, C. Jagadish, L. M. Smith, *Nano Lett.* **2007**, *7*, 588.
[19] S. A. Dayeh, E. T. Yu, D. Wang, *Nano Lett.* **2007**, *7*, 2486.
[20] L. C. Chuang, M. Moewe, S. Crankshaw, C. Chang-Hasnain, *Appl. Phys. Lett.* **2008**, *92*, 013121.
[21] D. H. Reep, S. K. Ghandhi, *J. Electrochem. Soc.* **1984**, *131*, 2697.
[22] A. M. S. El Ahl, M. He, P. Zhou, G. L. Harris, L. Salamanca-Riba, F. Felt, H. C. Shaw, A. Sharma, M. Jah, D. Lakins, T. Steiner, S. N. Mohammad, *J. Appl. Phys.* **2003**, *94*, 7749.
[23] K. Ikejiri, J. Noborisaka, S. Hara, J. Motohisa, T. Fukui, *J. Cryst. Growth* **2007**, *298*, 616.
[24] D. H. Reep, S. K. Ghandhi, *J. Electrochem. Soc.* **1983**, *130*, 675.
[25] D. K. Biegelsen, R. D. Bringans, J. E. Northrup, L.-E. Swartz, *Phys. Rev. Lett.* **1990**, *65*, 452.
[26] T. Hayakawa, M. Morishima, S. Chen, *Appl. Phys. Lett.* **1991**, *59*, 3321.
[27] J. Hu, T. W. Odom, C. M. Lieber, *Acc. Chem. Res.* **1999**, *32*, 435.
[28] S. Kodambaka, J. Tersoff, M. C. Reuter, F. M. Ross, *Science* **2007**, *316*, 729.
[29] K. A. Dick, K. Deppert, M. W. Larsson, T. Martensson, W. Seifert, L. R. Wallenberg, L. Samuelson, *Nat. Mater.* **2004**, *3*, 380.
[30] K. A. Dick, K. Deppert, L. S. Karlsson, W. Seifert, L. R. Wallenberg, L. Samuelson, *Nano Lett.* **2006**, *6*, 2842.
[31] J. Johansson, L. S. Karlsson, C. P. T. Svensson, T. Mårtensson, B. A. Wacaser, K. Deppert, L. Samuelson, W. Seifert, *Nat. Mater.* **2006**, *5*, 574.
[32] Y. Hao, G. Meng, Z. L. Wang, C. Ye, L. Zhang, *Nano Lett.* **2006**, *6*, 1650.
[33] Q. Li, X. Gong, C. Wang, J. Wang, K. Ip, S. Hark, *Adv. Mater.* **2004**, *16*, 1436.
[34] D. T. J. Hurle, *J. Cryst. Growth* **1995**, *147*, 239.
[35] H. Okamoto, T. B. Massalski, in *Binary Alloy Phase Diagrams*, Vol. 1, 1st ed, (Ed: T. B. Massalski,), ASM Int., Materials Park, OH **1986**, pp. 191–192.
[36] M. Copel, M. C. Reuter, E. Kaxiras, R. M. Tromp, *Phys. Rev. Lett.* **1989**, *63*, 632.
[37] E. I. Givargizov, *J. Cryst. Growth* **1973**, *20*, 217.
[38] V. Swaminathan, D. L. V. Haren, J. L. Zilko, P. Y. Lu, N. E. Schumaker, *J. Appl. Phys.* **1985**, *57*, 5349.
[39] L. V. Titova, T. B. Hoang, J. M. Yarrison-Rice, H. E. Jackson, Y. Kim, H. J. Joyce, Q. Gao, H. H. Tan, C. Jagadish, X. Zhang, J. Zou, L. M. Smith, *Nano Lett.* **2007**, *7*, 3383.
[40] E. H. Bogardus, H. B. Bebb, *Phys. Rev.* **1968**, *176*, 993.
[41] R. C. C. Leite, A. E. DiGiovanni, *Phys. Rev.* **1967**, *153*, 841.
[42] Y. M. K. Tanaka, H. Uchiki, K. Nakazawa, H. Araki, *Phys. Status Solidi A* **2006**, *203*, 2891.
[43] D. G. Thomas, J. J. Hopfield, W. M. Augustyniak, *Phys. Rev.* **1965**, *140*, A202.
[44] a) B. J. Skromme, T. S. Low, T. J. Roth, G. E. Stillman, J. K. Kennedy, J. K. Abrokwah, *J. Electron. Mater.* **1983**, *12*, 433. b) B. J. Skromme, G. E. Stillman, *Phys. Rev. B* **1984**, *29*, 1982.
[45] P. D. Dapkus, H. M. Manasevit, K. L. Hess, T. S. Low, G. E. Stillman, *J. Cryst. Growth* **1981**, *55*, 10.
[46] T. F. Kuech, E. Veuhoff, *J. Cryst. Growth* **1984**, *68*, 148.
[47] D. C. Reynolds, D. N. Talwar, M. O. Manasreh, C. E. Stutz, *Phys. Rev. B* **1993**, *47*, 13304.
[48] A. L. Gurskii, S. V. Voitikov, *Solid State Commun.* **1999**, *112*, 339.
[49] a) Z. H. Lu, M. C. Hanna, D. M. Szmyd, E. G. Oh, A. Majerfeld, *Appl. Phys. Lett.* **1990**, *56*, 177. b) M. Ciorga, L. Bryja, J. Misiewicz, R. Paszkiewicz, M. Panek, B. Paszkiewicz, M. Tlaczala, *Adv. Mater. Opt. Electron.* **1998**, *8*, 9.
[50] H. Mori, S. Takahashi, *Jpn. J. Appl. Phys. Part 2* **1984**, *23*, L877.
[51] L. C. Chuang, M. Moewe, C. Chase, N. P. Kobayashi, C. Chang-Hasnain, S. Crankshaw, *Appl. Phys. Lett.* **2007**, *90*, 043115.
[52] Y. Kim, H. J. Joyce, Q. Gao, H. H. Tan, C. Jagadish, M. Paladugu, J. Zou, A. A. Suvorova, *Nano Lett.* **2006**, *6*, 599.
[53] J. Noborisaka, J. Motohisa, S. Hara, T. Fukui, *Appl. Phys. Lett.* **2005**, *87*, 093109.